Article:
Tubman, E. R., Scott, R. H. H., Doyle, Hugo W. et al. (14 more authors) (2017) Time evolution and asymmetry of a laser produced blast wave. Physics of Plasmas. 103124. ISSN: 1089-7674

https://doi.org/10.1063/1.4987038

Time evolution and asymmetry of a laser produced blast wave

E. R. Tubman, R. H. H. Scott, H. W. Doyle, J. Meinecke, H. Ahmed, R. A. B. Alraddadi, R. Bolis, J. E. Cross, R. Crowston, D. Doria, D. Lamb, B. Reville, A. P. L. Robinson, P. Tzeferacos, M. Borghesi, G. Gregori, and N. C. Woolsey

Citation: Physics of Plasmas **24**, 103124 (2017);

View online: https://doi.org/10.1063/1.4987038

View Table of Contents: http://aip.scitation.org/toc/php/24/10

Published by the American Institute of Physics

Time evolution and asymmetry of a laser produced blast wave

E. R. Tubman,[1] R. H. H. Scott,[2] H. W. Doyle,[3] J. Meinecke,[3] H. Ahmed,[4] R. A. B. Alraddadi,[1] R. Bolis,[3] J. E. Cross,[3] R. Crowston,[1] D. Doria,[4] D. Lamb,[5] B. Reville,[4] A. P. L. Robinson,[2] P. Tzeferacos,[5] M. Borghesi,[4] G. Gregori,[3] and N. C. Woolsey[1]
[1]*York Plasma Institute, Department of Physics, University of York, York YO10 5DD, United Kingdom*
[2]*Central Laser Facility, STFC Rutherford Appleton Laboratory, Harwell, Oxford, Didcot OX11 0QX, United Kingdom*
[3]*Department of Physics, University of Oxford, Oxford OX1 2JD, United Kingdom*
[4]*Department of Physics, Queen's University, Belfast BT7 1NN, United Kingdom*
[5]*Department of Astronomy and Astrophysics, University of Chicago, Chicago, Illinois 60637, USA*

(Received 8 June 2017; accepted 28 September 2017; published online 13 October 2017)

Studies of a blast wave produced from carbon rods and plastic spheres in an argon background gas have been conducted using the Vulcan laser at the Rutherford Appleton Laboratory. A laser of 1500 J was focused onto these targets, and rear-side observations of an emission front were recorded using a fast-framing camera. The emission front is asymmetrical in shape and tends to a more symmetrical shape as it progresses due to the production of a second shock wave later in time, which pushes out the front of the blast wave. Plastic spheres produce faster blast waves, and the breakthrough of the second shock is visible before the shock stalls. The results are presented to demonstrate this trend, and similar evolution dynamics of experimental and simulation data from the FLASH radiation-hydrodynamics code are observed. https://doi.org/10.1063/1.4987038

I. INTRODUCTION

When the sudden point release of energy into a homogeneous medium creates a pressure driven supersonic shock wave, it propagates out into the surrounding medium in ideal conditions.[1] A physical system can be approximated by this model when the temporal and spatial scales are large compared to those associated with the energy release and the piston mass is negligible compared to the shocked mass.[2] Such shock waves, known as blast waves, are common in astrophysics, and blast wave dynamics are used to predict supernova remnant evolution.[3,4] These disturbances and associated shocks are readily created with high energy, intense lasers, enabling a detailed laboratory study of astrophysical relevant topics such as shock driven radiative instabilities,[5] secondary shock formation,[6] and the seeding[7] and amplification[8] of galactic magnetic fields. Furthermore, the scale-invariance of blast waves and application of ideal magneto-hydrodynamics to experiment[9] enable direct comparison of small scale (mm-sized and sub-micro-second) laboratory experiments with astronomical systems which have spatiotemporal scales many orders of magnitude larger.[10,11] Instabilities and magnetic fields are seeded from structures or asymmetries in shocks, and with high power laser facilities and fast camera systems, it is possible to control the asymmetry and monitor the evolution on a single shot. The understanding of the effect of target geometry and the development of the shape of the asymmetry are discussed within this report.

In Sec. II, we first describe the experimental setup designed to create asymmetric blast waves and the use of a fast framing camera to study the blast wave trajectory and asymmetry. Section III contains a detailed analysis of the fast framing camera results, including detailed comparisons with radiation-hydrodynamics simulations. We use two different target designs: a carbon rod and a hollow plastic sphere to assist in the understanding of the blast wave launch dynamics. The work is concluded in Sec. IV.

II. EXPERIMENTAL SETUP

This experiment was carried out using the Vulcan laser in Target Area West (TAW). Six infrared beams of 2 ns duration, with a total energy of 1.5 kJ, were clustered to a single, 300 μm diameter focal spot. This illuminated either a 500 μm diameter carbon rod target or a 2 mm diameter hollow plastic sphere target. The laser beams were organized on an arc in 3 sets of pairs at $\pm 25^\circ$ and 0° to the horizontal axis. The target was enclosed in a chamber containing a uniform background gas of argon at a pressure of 0.7 mbar. A schematic of the setup is shown in Fig. 1. The interaction of the laser with the target creates a rapidly expanding ablation plasma, the radiation from which ionises the surrounding gas. The ablating plasma acts as a piston on the surrounding medium driving a shock which evolves into a blast wave.

In addition to a magnetic induction coil or B-dot which was used to monitor changing magnetic fields, the experiment was also equipped with a Specialised Imaging SIM16 camera[12] timed to take sixteen self-emission frames of the blast wave up to 1 μs after the laser shot. This allowed prompt on-shot feedback of the spatial and temporal evolution of the blast wave. The camera uses a single optical line and is fitted with 16 independent CCD sensors coupled to microchannel plates (MCP). The MCPs used a 5 ns gate width and had separately programmable delays. The camera was filtered using a 620 ± 10 nm optical bandpass filter.

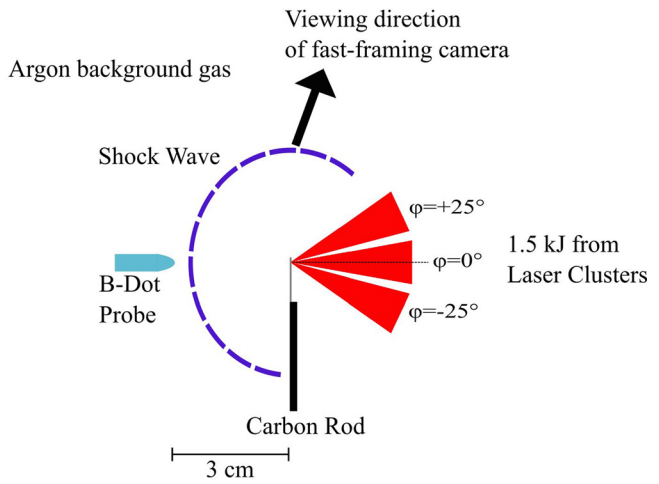

FIG. 1. A diagram of the experimental set-up for producing a blast wave from a carbon rod and propagating out into an ambient background gas.

III. ANALYSIS

An example of a fast framing camera image of the 500 μm carbon rod in 0.7 mbar of argon is shown in Fig. 2. On this shot, the camera was configured to record emission from the blast wave and timed to avoid the intense emission during the laser-target interaction and to stop recording just after the front of the blast wave reaches the B-dot probe. Superimposed on the first frame are the initial position of the target (labelled "Carbon Rod"), the position and angle of the laser, and the location of an induction probe (labelled "B-dot probe"). In the first two frames (20 and 60 ns), the strong emission is observed from the carbon and argon plasma surrounding the carbon rod, with a particularly strong emission halo from the side of the target not irradiated by the laser, the rear surface. By the third frame, at 100 ns, a near hemispherical emission front with a sharp edge is apparent. Front-tracking analysis of the emission front perpendicular to the target, in the plane view of the camera, gives the velocity of the emission front to be travelling at 40 ± 5 km/s at 200 ns. This emission front expands with time, and by 620 ns, the last frame in Fig. 2 has expanded to 2.00 ± 0.05 cm.

Figure 3 shows the images produced from 2 mm hollow plastic spheres which have sides of thickness 10 μm. Using this different target geometry, the images demonstrate more clearly that there are two shock-like structures produced by the interaction. Superimposed on the first frame are the locations of the target, the laser, and the B-dot probe. On the frame at 260 ns, an emission front is highlighted by a green line and a second, brighter emission front is highlighted by a blue line. Both emission fronts are flatter than those observed in Fig. 2. Front-tracking analysis (see below) shows that the brighter emission-front is travelling at a slightly faster velocity of 70 ± 10 km/s at 260 ns, compared to the flatter shock's velocity of 50 ± 10 km/s. By 440 ns, the two structures are more separated and distinct, and both features are decelerating.

Interestingly, the emission fronts monitored in these shots are not spherical and have a flatter shape in the viewing plane, which can be seen more clearly using plastic spheres. The carbon rods produce a smoother, more spherical shock than plastic spheres, although the targets are driven using the same laser parameters. A feature of these experimental data, which is of particular importance to our understanding of the dynamics of the shock topology evolution, is consistent with the observation of a second structure punching through the wider flatter shock when using the plastic spherical targets. This second structure moves separately to the wider, flatter front and is still propagating outwards after 350 ns when the other appears to have stalled.

By tracking the emission front trajectory and geometry, it is possible to monitor the front evolution for different shots. Due to the complexity of the plastic sphere emission

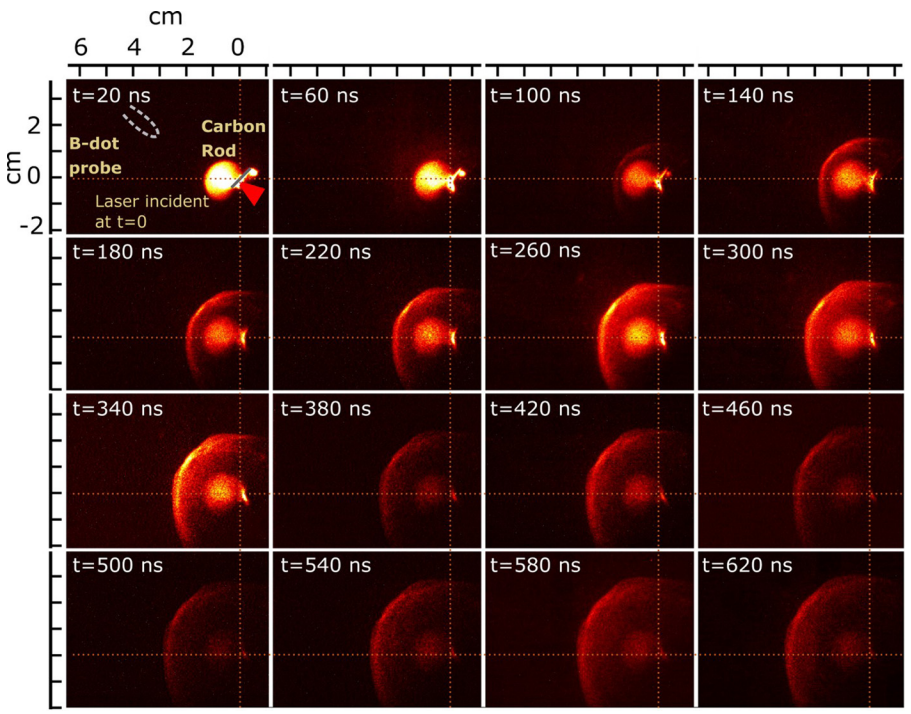

FIG. 2. The 16 frames produced on a single-shot by the SIM16 camera. Here, a blast wave has been produced from a carbon rod target, propagating out into a 0.7 mbar argon background gas. Temporal (recorded in the top left of each frame) and spatial (in cm around the top left corner frame) information can be gained from the shot. The dotted lines in each frame indicate the original target position (0,0). The images are taken with a 5 ns exposure.

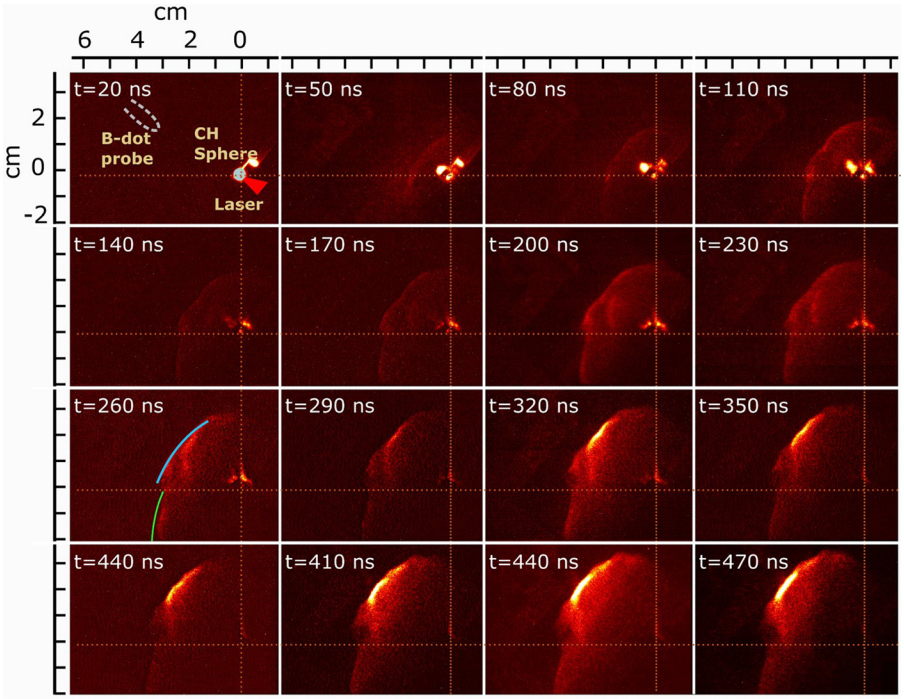

FIG. 3. Images collected using a plastic sphere target in a 0.7 mbar background argon gas. These images show two features being emitted from the shock, highlighted with the green and blue lines on the frame at 260 ns.

fronts, the mapping of the shock-like trajectories is challenging, and thus, no quantitative measurements of the asymmetry are presented. The asymmetry of the blast wave for carbon rod targets can be measured to understand the overall evolution and dependence on target geometry (Fig. 2). The observation and understanding of an asymmetrical blast wave shape are important, as it results in non-parallel temperature and density gradients, so the Biermann battery effect can generate magnetic fields.[13]

Each of the 16 self-emission frames collected in a shot was analysed to measure the outer shock edge position. Emission front position measurements are limited to ± 0.1 mm by the camera spatial resolution and uncertainty in spatial calibration. The position of the emission front was assumed to be the point of peak emission. There is also an additional error in estimating the position of the target origin which is ± 1 mm. This error would affect all the images on a single shot in the same manner so it has not been included in error analysis.

The simplest method to capture information about the asymmetrical shape of the emission front is to fit an ellipse to the points of peak emission. The fitting is applied to just the carbon rod targets due to the smoother profile of the shock being easier to track. An ellipse function with a tilt can be overlaid to the points across the emission front, with the function in Eq. (1),

$$1 = \frac{(x\cos\phi + y\sin\phi)^2}{R_a^2} + \frac{(x\cos\phi - y\sin\phi)^2}{R_b^2}, \qquad (1)$$

where x and y are the horizontal and vertical positions, $R_{a,b}$ are the major and minor axes, and ϕ is the tilt with respect to the x-axis. This enables an elliptical fit to the emission front with tilt, ϕ, as without applying any rotation to the frames, the ellipse will not be aligned along the horizontal or vertical axis. The tilt is observed to be relatively constant, with $\phi = 23 \pm 5^\circ$ over the duration of the shock propagation.

After fitting the ellipse, the ratio of R_a/R_b was plotted as a function of time in Fig. 4 for three shots with nominally the same conditions. Data from Fig. 2 are shown as green triangles. Here, R_b is the axis closest to that of the laser direction which, after analysis, is found to be the minor axis. The major axis R_a is perpendicular to this, in the direction closest to the target stalk axis. The ratio R_a/R_b is useful in describing the global asymmetry of the blast wave. A spherical blast-wave would have a ratio of 1, a blast-wave which propagates faster along the axis parallel to the laser would have a ratio <1 and a blast wave propagating faster in the orthogonal direction will have a ratio >1. From Fig. 4, we can see that the emission front has a ratio of 1.12 in early time (<100 ns), meaning that the expansion of the front is the largest in the direction perpendicular to the laser axis. This ratio decreases with time, tending towards a more symmetrical, spherical shock.

The minor axis (i.e., the axis aligned with the laser) length with time for a number of shots is plotted in Fig. 5.

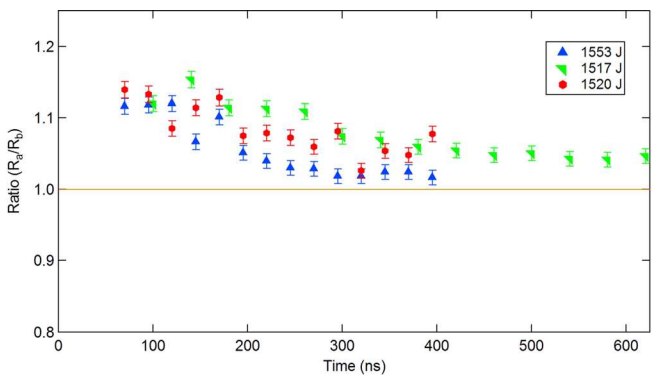

FIG. 4. The temporal evolution of the ratio of the major Ra to minor Rb axis of the ellipse for shots using carbon rods in 0.7 mbar Argon background gas and the laser energies, as specified, in a 2 ns pulse. This shows that at early time, the blast-waves are more asymmetric, tending toward sphericity.

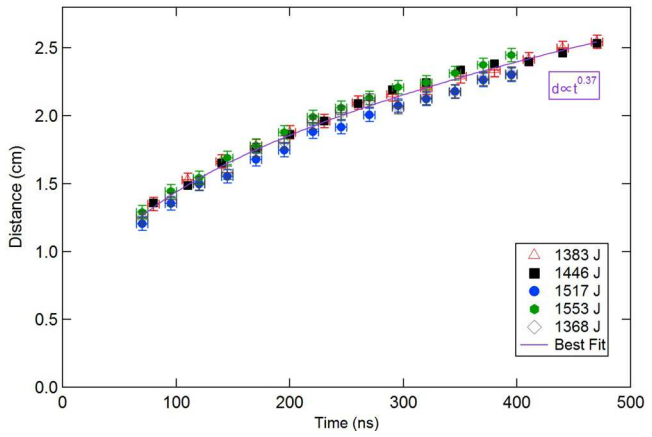

FIG. 5. The shock trajectory as measured at the ellipse minor axis (that aligned with the incoming laser axis) for various shots. The trajectory is consistent within the error across the various shots.

There is little variation between the three shots, suggesting that the differences between ellipticity for different shots reported in Fig. 4 are due to differences in expansion along the axis perpendicular to the laser direction. This may be the result of inconsistencies in laser pointing between shots. Additionally, the best fit line to the data appears to closely follow a Sedov-Taylor self-similar solution ($d \propto t^{0.4}$)[14,15] which could lead to future investigations of this matching over time.

The launch of a shock from a carbon rod and plastic spherical target was investigated using 2-dimensional FLASH radiation-hydrodynamics simulations.[16–18] Adaptive mesh refinement was used in order to resolve the large spatial (2×2 cm box) and temporal (1 μs) scales while maintaining acceptable spatial resolution (10 μm) where required. In the simulations, cylindrical symmetry was assumed,[19] with the spherical CH shell, represented by a hollow hemisphere on-axis. In the following discussion and figures, the x-axis is the radial direction, with $x = 0$ being the axis of symmetry.

In the simulations, the laser is incident from below the x-axis, parallel to the y-axis. Spot-sizes, intensities, powers, and pulse shapes were as per the experiment. Simulations showing the peak radiation front including the emission range observed by the optical camera can be compared with the experimental data. Figure 6 shows simulations run using plastic spheres as targets. The plastic spheres are a good example for demonstrating the emergence of the two asymmetrical fronts in a single interaction. At early times, the front is smooth, until 56 ns when a smaller structure punches through the top of the hotter, denser central target material. By 94 ns, the two structures become more pronounced. This supports the experimental data for plastic spheres where these two features evolve on much shorter timescales than for carbon rods.

These simulations reveal how the asymmetrical emission front shape is the result of two shocks. Each shock is driven by a different mechanism; a cartoon of these mechanisms is shown in Fig. 7. An initial shock expands out around the target. This is produced within the Argon background plasma by material ablated from the front-side of the target. A second shock is driven through the target by the laser. The shock propagating through the target appears later in time, as it travels more slowly within the denser target material than the shock propagating through the low-density Argon background chamber fill. Eventually, it breaks out

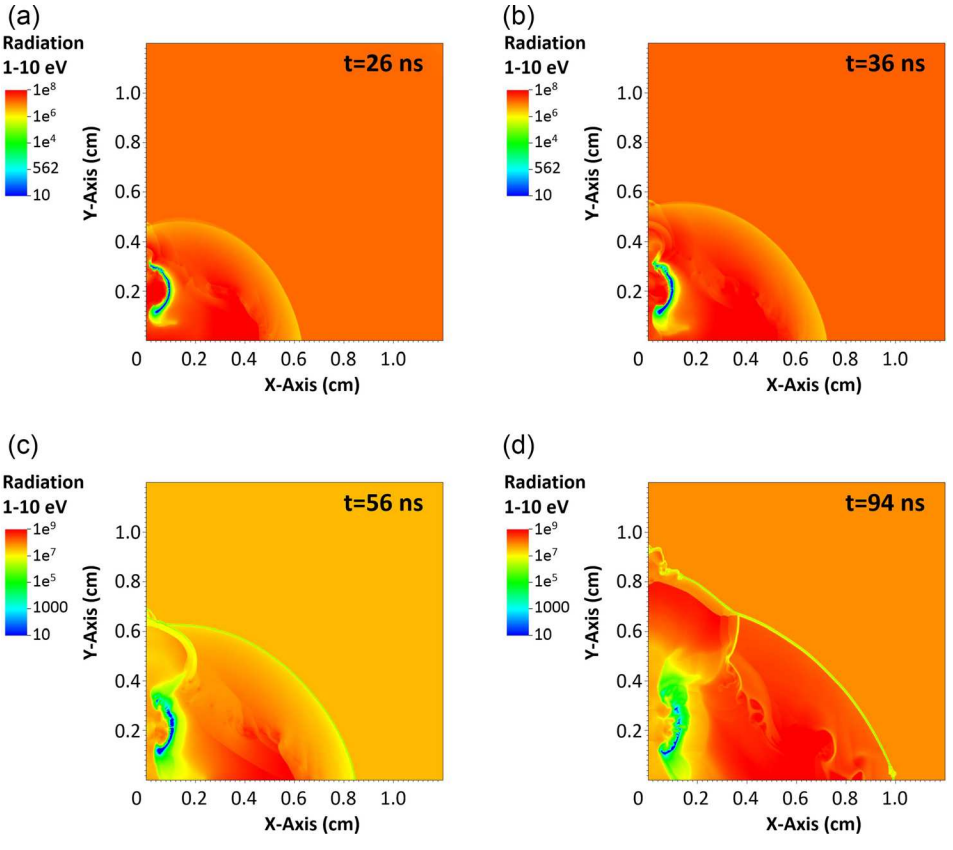

FIG. 6. A 2 D simulation in FLASH of a 2 mm plastic sphere producing a blast wave, where the production of two shock waves is more visible. These simulations show the intensity (arb. units) of the radiation between 1 and 10 eV, which will include the energy range the optical camera is able to image in the experiment.

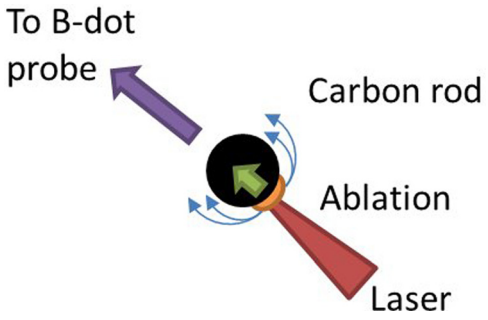

FIG. 7. A diagram showing the production of two shocks from the carbon rod. The blue arrows show the first shock produced from the ablated material expanding around the end and sides of the target. The green arrow shows the second shock through the target. The purple arrow gives the direction to the B-dot probe.

from the target rear side. When it emerges, it is faster travelling than the first shock and, under the right conditions, catches up with the slower shock.

As the two shocks merge, the second shock pushes the first shock out further in the direction of the laser axis, and so whilst the sides of the shock are slowing down even further, the front is able to expand more and create a more symmetrical shock. This is the reason for having a decrease in the ellipticity like that shown in Fig. 4.

Similar dynamics causing two shocks to be produced in an interaction have been observed by Tzeferacos *et al.*[18] and Gregori *et al.*[7] In the former, two fronts are observed in FLASH simulations and one is suggested to be due a shock launched into the background gas and the second from the target material expanding behind. In the latter reference, the B-dot probe signal showed measurements of two peaks in the magnetic field strengths, and this is postulated to be from the target ejecta material. However, in light of the results presented in this paper, we are able to further describe the generation of the two shock structures and discuss the evolution in more detail.

Comparisons between simulation of the plastic spheres and carbon rod target (as shown in Fig. 8) show that in the case of the plastic spheres, the two shocks cross much earlier in time and progress even further, creating an asymmetrical shock but with the minor and major axes flipped by 90°. These go on to create a more irregular shock before the emission reduces below the camera threshold. The carbon rod shock evolution has already stalled before the second shock has caught up with the first; therefore, the two shocks never cross and flip the ellipse's axes.

The plots in Fig. 8 also show the two hemispherical peaks in radiation intensity, which are most apparent at 231 ns and separated by about 0.5 cm in the x-axis direction at $y = 0$. These would be more difficult to observe experimentally due to the 3 D nature of the experiment and viewing angle of the camera, so we are unable to distinguish the separate shocks. Between the two fronts in the simulations, it appears that the flow is also becoming more turbulent. By 361 ns, these two fronts have started to merge and the emission front is becoming disrupted towards the outer edges. As previously discussed, the limited spatial resolution of the imaging system means that the camera will not be able to resolve these small scale features. At early time, these shocks expand out furthest in the direction perpendicular to the laser axis (y-axis). The qualitative and quantitative shock front

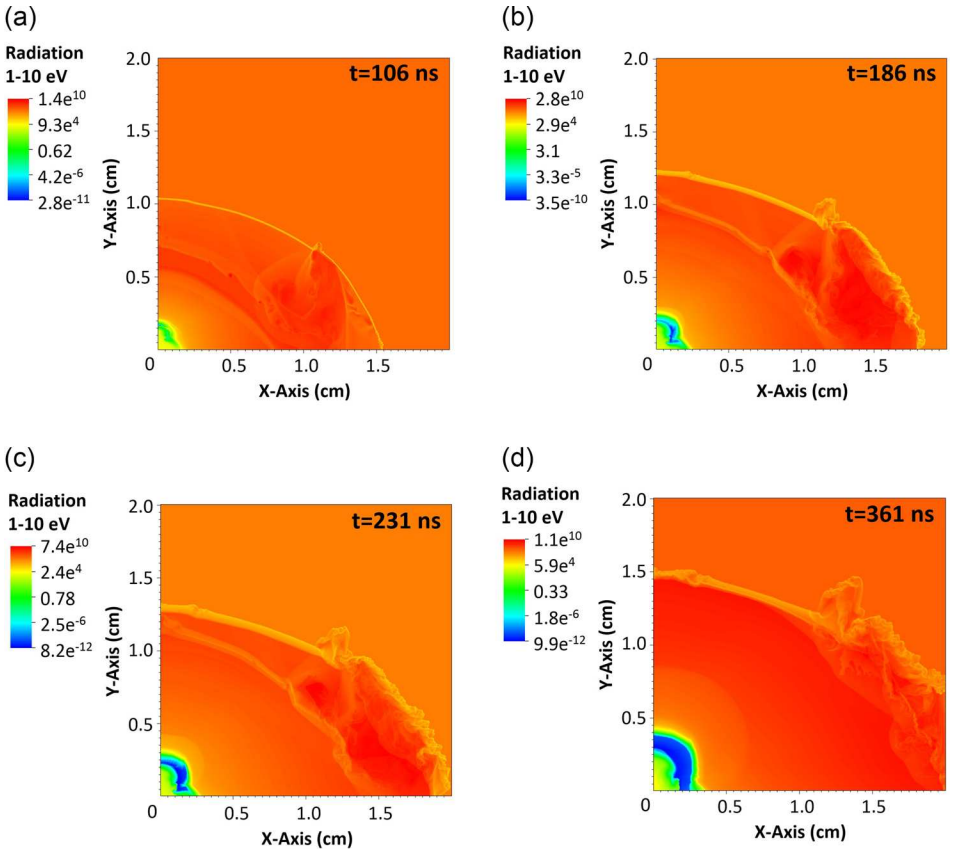

FIG. 8. 2 D simulations using FLASH of a carbon spherical target producing a blast wave. A map of the 1–10 eV spectral emission at various time intervals is shown. The cylindrical symmetry required approximation of the carbon rod to be represented as a circular disc revolved around the axis of symmetry.

evolution of the simulations closely matches those measured experimentally.

When viewing the experimental data of the carbon rods, the emission front is observed to be much smoother as the two shocks have slowed down earlier in time than for plastic spheres and move together without changing the separation between the two shocks. The reason for the difference in the overall shock velocities of the targets is due to the density of the materials and the absorption of laser energy. The shocks follow a Sedov-Taylor solution[14,15] in their evolution, and thus, the energy density and therefore velocity decrease as the shock expands. The reason for the difference in the overall shock velocities is due to the individual target densities and absorption of laser energy. The carbon shocks slow but faster than the plastic as they absorb a smaller fraction of the laser energy initially and so reach a lower energy density sooner than the plastic. Eventually, the shocks will move together, and this is a common phenomenon, for example, in the multi-shock NIF design, where multiple shocks merge at or near the inner DT ice surface. Prior to the merging, the spatially separated shocks have different local characteristics and encounter different upstream and downstream fluid parameters leading to distinct velocities. At the point of the shock merging, there is no distinction between the fluid characteristics associated with the initially separate shocks; they become one. Subsequently, the shocks must propagate as one forward shock and a second backward travelling rarefaction wave. In the plastic spheres, the second shock wave catches up with the first whilst it still has a larger speed than the first shock due and so it will break through the first and they will travel more independently. The production of these two features is more obvious using targets such as plastic spheres and could potentially be enhanced further by using other target geometries.

These experimental and simulation results provide a more complete picture of the asymmetry origin observed in laboratory shock waves and their temporal evolution. Due to the associated non-parallel gradients in temperature and density, these will generate magnetic fields through the Biermann battery effect. Furthermore, the simulation results also suggest the creation of turbulent flows in the region behind the shock front(s) (Fig. 8), although it was not possible to resolve these experimentally.

IV. CONCLUSIONS

From the experimental results, we have observed the production of two asymmetrical blast waves from the self-emission in the ambient background gas. Using an ellipse fitting procedure, we infer that to the shock front, asymmetry decreases over time. Through a combination of experimental data analysis and numerical simulations, we argue that this is due to a second shock wave being produced later in time as the piston emerges through the target. In carbon rods, this shock pushes the overall blast wave shape to being more symmetrical. For plastic spheres, conversely, the two shocks become quite separate later in time due to a faster second shock, causing a more irregular overall shape.

This analysis may be of interest to experiments investigating turbulence in shock waves and the generation of magnetic fields. The shock waves produced through the target tend to be more consistent across different shots, whereas the shock waves perpendicular to the laser axis have more shot variability due to the target and laser setup. The fields measured at the shock front opposite to the laser axis should be more repeatable and consistent shot to shot. However, the turbulence, occurring at the emission edges perpendicular to the laser axis, produced by targets such as carbon rods may have other effects such as amplification on the fields which could be further investigated.

In conclusion, the framing camera is an effective tool for observing an interaction where shock features are created and developed over nanosecond time scales. The asymmetry of a blast wave emerging from the rear-side of the target is argued to be due to two shock waves and may influence other measurements made, such as the magnetic fields, depending on the stage of development of the two waves.

ACKNOWLEDGMENTS

The authors acknowledge the funding from the ERC under the EUs FP7 (FP7/2007–2013)/ERC Grant Agreement No. 256973 and by the EPSRC and the STFC (Grant Nos. EP/K022415/1 and EP/L002221/1) and InvestNI PoC. This work was also supported in part at the University of Chicago by the U.S. DOE NNSA ASC through the Argonne Institute for Computing in Science under FWP 57789 and the U.S. DOE Office of Science through Grant No. DE- SC0016566. The software used in this work was developed in part by the DOE NNSA ASC- and DOE Office of Science ASCR-supported Flash Center for Computational Science at the University of Chicago. We would also like to thank the CLF staff for their assistance in the running of the experiment at the Rutherford Appleton Laboratories.

[1]L. I. Sedov, *Similarity and Dimensional Methods in Mechanics* (Elsevier Science, 1959).
[2]Y. B. Zel'dovich and Y. P. Raizer, *Physics of Shock Waves* (Dover Publications, Inc., 2003).
[3]J. P. Ostriker and C. F. McKee, Rev. Mod. Phys. **60**, 1 (1988).
[4]J. Sanz, S. E. Bouquet, C. Michaut, and J. Miniere, Phys. Plasmas **23**, 062114 (2016).
[5]J. Grun, J. Stamper, C. Manka, J. Resnick, R. Burris, J. Crawford, and B. H. Ripin, Phys. Rev. Lett. **66**, 2738 (1991).
[6]J. F. Hansen, M. J. Edwards, D. H. Froula, G. Gregori, A. D. Edens, and T. Ditmire, Phys. Plasmas **13**, 022105 (2006).
[7]G. Gregori, A. Ravasio, C. D. Murphy, K. Schaar, A. Baird, A. R. Bell, A. Benuzzi-Mounaix, R. Bingham, C. Constantin, R. P. Drake *et al.*, Nature **481**, 480 (2012).
[8]J. Meinecke, H. W. Doyle, F. Miniati, A. R. Bell, R. Bingham, R. Crowston, R. P. Drake, M. Fatenejad, M. Koenig, Y. Kuramitsu *et al.*, Nat. Phys. **10**, 520 (2014).
[9]D. Ryutov, R. P. Drake, J. Kane, E. Liang, B. A. Remington, and W. M. Wood-Vasey, Astrophys. J. **518**, 821 (1999).
[10]D. D. Ryutov, B. A. Remington, H. F. Robey, and R. P. Drake, Phys. Plasmas **8**, 1804 (2001).
[11]J. E. Cross, B. Reville, and G. Gregori, Astrophys. J. **795**, 59 (2014).
[12]S. Imaging, Framing cameras, 2016.
[13]R. M. Kulsrud and E. G. Zweibel, Rep. Prog. Phys. **71**, 046901 (2008).
[14]L. I. Sedov, Prikl. Mat. Mekh. **10**, 241 (1946).
[15]G. Taylor, Proc. R. Soc. A: Math., Phys. Eng. Sci. **200**, 235 (1950).

[16]B. Fryxell, K. Olson, P. Ricker, F. X. Timmes, M. Zingale, D. Q. Lamb, P. MacNeice, R. Rosner, J. W. Truran, and H. Tufo, Astrophys. J. Suppl. Ser. **131**, 273 (2000).
[17]A. Dubey, K. Antypas, M. K. Ganapathy, L. B. Reid, K. Riley, D. Sheeler, A. Siegel, and K. Weide, Parallel Comput. **35**, 512 (2009).
[18]P. Tzeferacos, M. Fatenejad, N. Flocke, C. Graziani, G. Gregori, D. Lamb, D. Lee, J. Meinecke, A. Scopatz, and K. Weide, High Energy Density Phys. **17**, 24 (2015).
[19]P. Tzeferacos, M. Fatenejad, N. Flocke, G. Gregori, D. Lamb, D. Lee, J. Meinecke, A. Scopatz, and K. Weide, High Energy Density Phys. **8**, 322 (2012).